FIGGIS, B. N., GERLOCH, M. & MASON, R. (1964). *Acta Cryst.* **17**, 506–508.
FIGGIS, B. N., MASON, R., SMITH, A. R. P. & WILLIAMS, G. A. (1979). *J. Am. Chem. Soc.* **101**, 3673–3675.
FIGGIS, B. N., MASON, R., SMITH, A. R. P. & WILLIAMS, G. A. (1980). *Acta Cryst.* B**36**, 509–512.
FIGGIS, B. N., REYNOLDS, P. A. & WILLIAMS, G. A. (1980). *J. Chem. Soc. Dalton Trans.* In the press.
FIGGIS, B. N., REYNOLDS, P. A., WILLIAMS, G. A., MASON, R., SMITH, A. R. P. & VARGHESE, J. N. (1980). *J. Chem. Soc. Dalton Trans.* In the press.
International Tables for X-ray Crystallography (1968). Vol. III, pp. 197–199. Birmingham: Kynoch Press.
International Tables for X-ray Crystallography (1974). Vol. IV, pp. 270–271. Birmingham: Kynoch Press.
JOHNSON, C. K. (1965). *ORTEP*. Report ORNL-3794. Oak Ridge National Laboratory, Tennessee.
LARSON, A. C. (1967). *Acta Cryst.* **23**, 664–665.
LE PAGE, Y. & GABE, E. J. (1979). *Acta Cryst.* A**35**, 73–78.
MOORE, F. H. & COLYVAS, K. (1980). Unpublished data.
POWELL, H. M. & WELLS, A. F. (1935). *J. Chem. Soc.* pp. 359–362.
REYNOLDS, P. A., FIGGIS, B. N. & WHITE, A. H. (1981). *Acta Cryst.* In the press.
SCHOMAKER, V. & TRUEBLOOD, K. N. (1968). *Acta Cryst.* B**24**, 63–76.
STEWART, J. M. (1976). The XRAY 76 system. Tech. Rep. TR-446. Computer Science Center, Univ. of Maryland, College Park, Maryland.
WILLIS, B. T. M. & PRYOR, A. W. (1975). *Thermal Vibrations in Crystallography*, pp. 232–241. Cambridge Univ. Press.

Acta Cryst. (1980). B**36**, 2897–2902

The Structure of $Ba_xTi_{8-2x}Ga_{10+2x}O_{31}$

BY L. A. BURSILL*

Department of Physical Chemistry, Lensfield Road, Cambridge CB2 1EP, England

(*Received* 4 *December* 1979; *accepted* 21 *July* 1980)

Abstract

The crystal structure of $Ba_xTi_{8-2x}Ga_{10+2x}O_{31}$ is studied by high-resolution (3 Å) electron microscopy. The tunnel structure contains elements of the hollandite, rutile and β-gallia structure types, intergrown coherently to produce a tetragonal unit cell with $a_1 = a_2 = 19{\cdot}1$ and $c = 2{\cdot}96$ Å. Computer simulation of the images shows that a structural model, derived by intuitive interpretation of an image recorded near the Scherzer defocus condition, gives a good image match with experimental images, provided full N-beam multislice techniques are employed.

1. Introduction

The structural relationships between hollandite, rutile and a number of other titanate structures suggested (Bursill, 1979*a*) that hollandite-type tunnels could be produced at orthogonal intersections of $\{210\}\langle\frac{1}{2}\frac{1}{2}\frac{1}{2}\rangle$ crystallographic shear planes in rutile. Examples of 25 distinct defect intersection structures were found in a study of Mg- and Ga-doped rutiles (Bursill, 1979*b*). Now the structure building element common to both hollandite and β-Ga_2O_3 is a double-string of edge-shared $[MO_6]$ octahedra parallel to c_{holl} or b_β (*cf.* Figs. 1*b* and 4*b* in Bursill, 1979*a*) and it was therefore predicted that Ba-hollandites containing Ga^{3+} in the framework would be relatively more stable than those containing other trivalent cations, *e.g.* Mn, Ti, Al, which do not adopt the β-Ga_2O_3-type structure. We therefore attempted to prepare hollandites having formulae $Ba_xTi_{8-2x}Ga_{2x}O_{16}$ with $x < 0{\cdot}5$. A sample of mean stoichiometry $x = 0{\cdot}5$ was found to contain two phases. The major phase was a hollandite with $x = 0{\cdot}8$ which exhibited incommensurate superlattice ordering of Ba^{2+} ions along the hollandite tunnels (Bursill, 1979*c*; Bursill & Grzinic, 1980). The minor component exhibited a $19{\cdot}1 \times 19{\cdot}1$ Å tetragonal unit cell and this unknown structure became the subject of this paper. It provided a good test object for a goniometer developed for use in objective-lens pole pieces having spherical-aberration coefficient $C_s = 0{\cdot}7$ mm (Bursill, Spargo, Wentworth & Wood, 1979).

2. Experimental

Weighed amounts of finely powdered Ga_2O_3, TiO_2 and $BaCO_3$ (Koch-Light, 4N) having overall stoichiometry

* On leave from: School of Physics, The University of Melbourne, Parkville, Victoria 3052, Australia.

0567-7408/80/122897-06$01.00

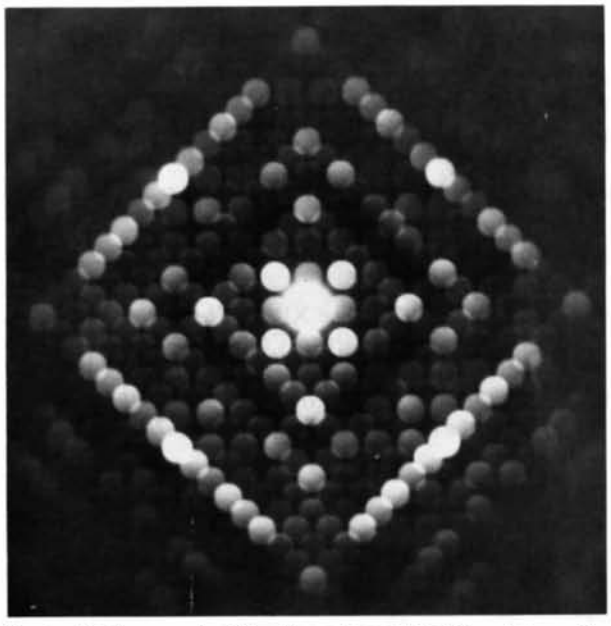

Fig. 1. [001] zone axis diffraction pattern of $Ba_xTi_{8-2x}Ga_{10+2x}O_{31}$, showing incident-beam divergence used for imaging. Note the fourfold symmetry with $a_1 = a_2 = 19{\cdot}1$ Å.

$Ba_{0{\cdot}5}GaTi_7O_{16}$ ($+CO_2\uparrow$) were mixed and pressed into a pellet. The pellet was wrapped in Pt foil and a solid-state reaction was carried out for 2 h at 1373 K. The pellet was reground and further reacted at 1473 K for 12 h. Thin fracture fragments of the resulting polycrystalline mass were obtained by grinding in an agate mortar under chloroform and these were deposited on to carbon-lace support films.

The optical parameters of the objective-lens pole-pieces were $C_s = 0{\cdot}7$ mm, chromatic-aberration coefficient $C_c = 1{\cdot}05$ mm and focal length $f_o = 1{\cdot}35$ mm. Standard hairpin filaments were used in the cool-beam Wehnhelt cap of a Jeol 100C electron microscope. The goniometer allows tilts of up to $\pm 15°$ about two mutually perpendicular axes, with X and Y translations of ± 1 mm. Crystals were precisely aligned with the short axis ($c = 2{\cdot}96$ Å) parallel to the incident electron beam. A typical diffraction pattern, showing the imaging conditions, is given in Fig. 1, from which the incident-beam divergence was estimated to be 0·6 mrad. High-resolution images were recorded using electron-optical magnifications of 540 000× to 1 000 000×. Care was taken to minimize space charge and thermal-energy spread in the gun, by optimizing the gun bias setting. Exposure times ranged from 2 to 20 s for Kodak 4463 film, developed for 5 min in D19 developer.

3. Results

Fig. 2(*a*) shows an overall view of one crystal which was studied at length. Note the remarkable variation of image contrast with increasing distance from the crystal edge. It shows relatively simple contrast for the first three or four unit cells from the edge, shown enlarged in Fig. 2(*b*). The 19·1 Å^2 unit cell contains two large white regions, each of which is surrounded by four intense black blobs. These are linked together by less intense black blobs separated by ~3·2 Å. The remainder of the asymmetric unit is occupied by four less dense dark blobs within blocks of 5 or 6 white blobs having roughly rectangular 3 × 2 groupings. Adjacent blocks are rotated through 90°. In the thicker parts of the crystal these blocks degenerate into orthogonal pairs of white bars within a square of white blobs having edge $19{\cdot}1/\sqrt{2} = 13{\cdot}5$ Å and it is this periodicity, rather than the true unit cell of 19·1 Å, which tends to dominate the contrast for thicker crystalline regions. Note that the contrast near the crystal edge does not reappear in thicker regions. This behaviour is in marked distinction to the thickness periodicity observed for images of Si (or Ge) and H-Nb_2O_5 observed by Spence, O'Keefe & Iijima (1978). Fig. 3(*a*) to (*d*) shows four high-resolution images of the same thin edge obtained by varying the objective-lens defocus Δf. Intricate changes of contrast occur in both the thin and thicker parts of the crystal. The values of Δf were estimated experimentally by finding the minimum-contrast condition, which should occur for

$$\Delta f_{\rm mc} \simeq -\tfrac{1}{2}(\lambda C_s)^{1/2} \qquad (1)$$

(see Wilson, Bursill & Spargo, 1979) and then assigning Δf by using the manufacturer/supplier value of 35 Å per fine click of the objective-lens current control. These values were also checked by comparing the observed Fresnel-fringe edge contrast with periodic continuation calculations (Wilson *et al.*, 1979). Thus Fig. 3(*b*) is close to the optimally focused condition according to Scherzer's (1949) criterion with $\Delta f \sim -620$ Å and Fig. 3(*c*) is close to the minimum-contrast condition ($\Delta f \sim -254$ Å). Similarly, Figs. 3(*a*) and (*d*) were assigned values of $\Delta f = -1100$ and $+200$ Å respectively. We note that these Δf values strictly apply only at the crystal edge, since for wedge crystals the exit surface of the crystal may be inclined to the horizontal.

4. Structure resolution criteria

These are based on establishing an isomorphism (one-to-one correspondence) between image intensity and some property of the structure of the object; for example, the projected potential or charge density. However, in general there is a homomorphism (many-to-one correspondence) between black or white blobs on the image and the positions of some of the atoms or voids in the appropriate projection of the structure.

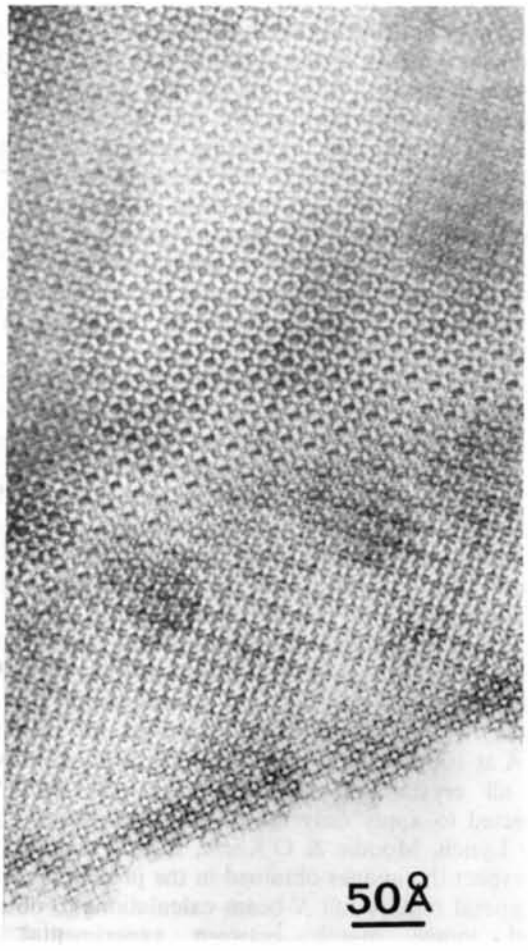

(*a*)

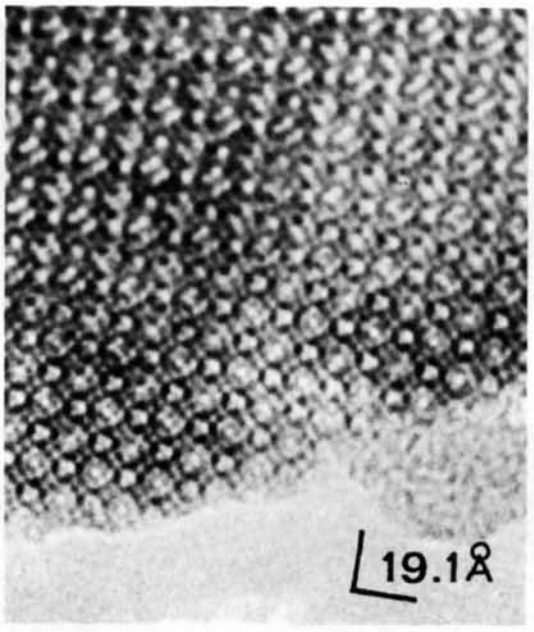

(*b*)

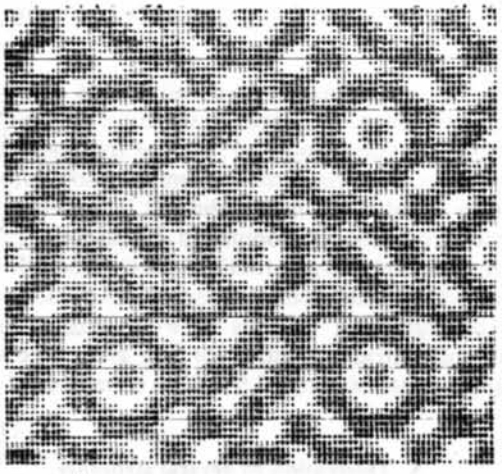

$H = 30$ Å

(*c*)

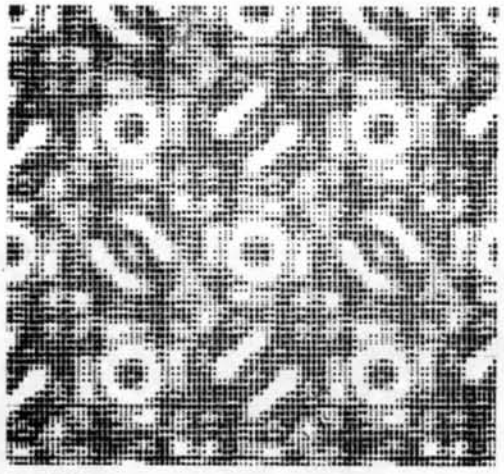

$H = 85$ Å

(*d*)

Fig. 2. (*a*) Overall view of the crystal used for structure determination. Note the remarkable variation of image contrast with increasing distance from the crystal edge. The simple (interpretable) edge contrast does not recur with thickness. (*b*) Enlargement of (*a*) showing edge contrast. (*c*), (*d*) Computer-simulated image match for thin ($H = 30$ Å, $R = 3$ Å, $\Delta f = -600$ Å) and thicker regions ($H = 85$ Å, $R = 3$ Å, $\Delta f = -600$ Å).

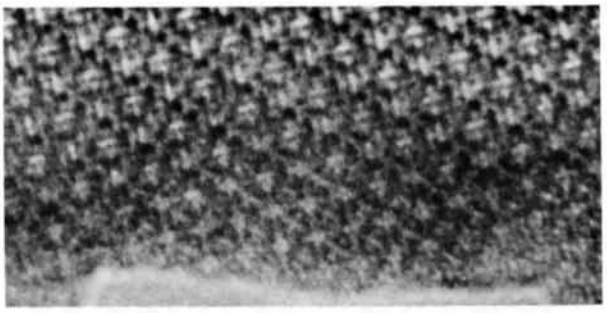

(*a*) ($\Delta f = -1100$ Å)

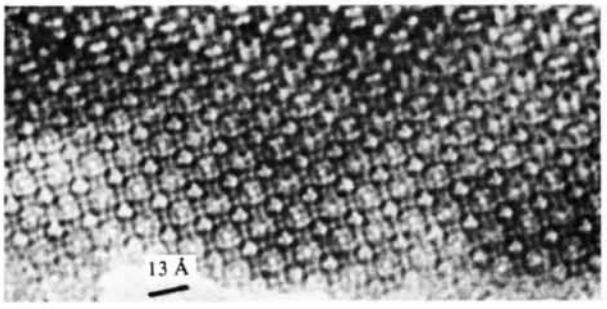

(*b*) ($\Delta f = -610$ Å)

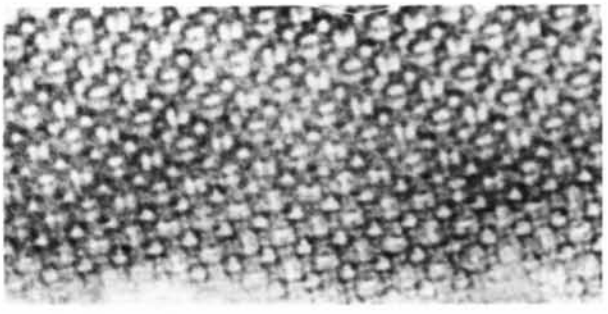

(*c*) ($\Delta f = -250$ Å)

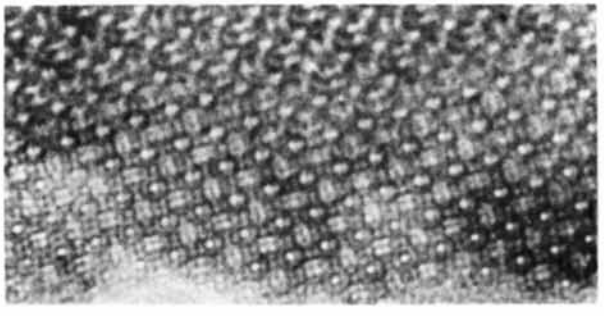

(*d*) ($\Delta f = 200$ Å)

Fig. 3. Through-focal series of images of the area of Fig. 2(*b*). Note the low contrast in (*c*) which is topologically very similar to the optimally defocused image (*b*).

There may be contrast reversals and/or origin shifts at particular settings of the objective-lens defocus, Δf, or crystal thickness. Thus for Si the image intensity apparently recurs periodically for increasing crystal thickness H and with increasing defocus Δf (Spence, O'Keefe & Kolar, 1977). For crystals having larger unit cells, when several hundreds of beams may be effective in forming the image, variations of image intensity with Δf and H are in general *not* periodic and many more homomorphisms exist between features of the image and the arrangement of the atoms in the crystal (see Fig. 2*a*).

Clearly, if there is to be rapid progress in a structure determination it is necessary to establish conditions for which there is an isomorphism between the positions of the atoms in the appropriate projection of the structure and the image intensity. Attempts have been made to define simple approximations whereby the image intensity is proportional to the projected potential of the crystal [the so-called Scherzer or weak-phase-object approximation, WPOA (Cowley, 1975)] or to the projected-charge-density approximation [the so-called PCDA (Lynch, Moodie & O'Keefe, 1975)]. These have limited ranges of applicability, as indicated in Fig. 2 of Lynch, Moodie & O'Keefe. However, for resolution ~3 Å at 100 kV and $C_s = 0{\cdot}7$ mm the WPOA is invalid for all crystal thicknesses whereas the PCDA is expected to apply only for crystal thicknesses <10 Å (see Lynch, Moodie & O'Keefe, Figs. 2 and 3). Thus we expect the images obtained in the present study will in general require full N-beam calculations to obtain a good image match between experimental and computer-simulated images. We note that the projected charge density is given by

$$\rho^p(x,y) = 16\pi^2 \sum_{hkl} F_{hkl} u^2 \exp(hXi + kYi), \qquad (2)$$

when the summation is over all beams effective in forming the image. F_{hkl} are the structure amplitudes for electrons (in volts) and X_i, Y_i are the fractional atomic coordinates. The truncated (or limited-resolution) PCD given by equation (2) is only directly interpretable if the atomic projection is dominated by atomic columns having relatively large atomic numbers and which are separated by interatomic distances <3 Å. Characteristic distinguishing features of PCD images are the minimum-contrast condition for Δf_{mc} given by equation (1) and a contrast reversal for Δf on either side of Δf_{mc}.

5. Derivation of crystal structure

The through-focal series of images shown in Fig. 3(*a*) to (*d*) does not clearly show all of the features expected for the PCD approximation. Fig. 3(*c*), which is close to the minimum-contrast condition [equation (1)], *i.e.* $\Delta f = -250$ Å, differs essentially from Fig. 3(*b*), which shows

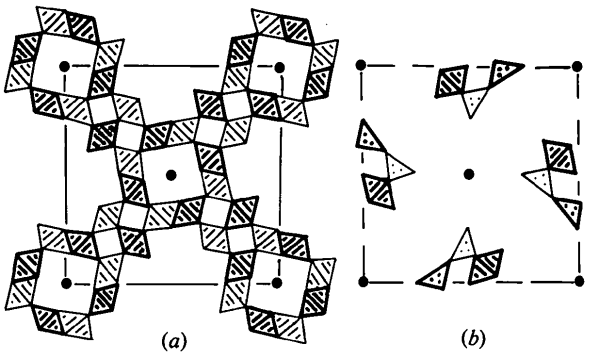

Fig. 4. (*a*) Hollandite-like tunnels and rutile-like framework deduced by assuming PCD approximation and intuitively interpreting Fig. 2(*b*). (*b*) Completion of the structure by insertion of β-gallia-type structural elements.

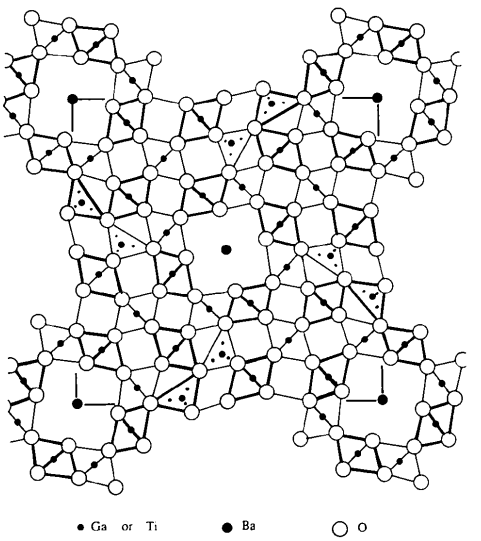

Fig. 5. [001] projection of $BaTi_6Ga_{12}O_{31}$ calculated using real atomic coordinates for hollandite-, rutile- and β-gallia-type structures.

the approximate optically defocused image (Δf = −610 Å), only in the contrast. It shows essentially the same topology but with very low contrast at the crystal edge. Fig. 3(*d*), which corresponds to $\Delta f \sim +200$ Å, shows quite different contrast detail which unfortunately is not a simple contrast reversal compared to Fig. 3(*b*, *c*). Similarly, Fig. 3(*a*), which corresponds to $\Delta f \sim -1100$ Å, shows new contrast features which cannot be explained using the PCD approximation. The observation that Figs. 3(*b*, *c*) show essentially the same topology with a lowering of contrast as Δf approaches the minimum-focus condition strongly suggested that the images approach the PCD approximation for -600 Å $< \Delta f < -200$ Å. A structural model was therefore derived by assuming the PCD approximation. This model was then used to compute through-focal and through-thickness series of images, using full *N*-beam multislice computation techniques, for comparison with the images shown in Figs. 2 and 3.

The large intense white blobs of Fig. 3(*b*) (also Fig. 2*b*) show contrast very similar to that obtained previously (Bursill & Wilson, 1977) for hollandite-type tunnels viewed along $\mathbf{c}_{holl}$. These would presumably contain Ba atoms. Six intense dark blobs link the intense white blobs. These have 3 × 2 rectangular arrays with blob spacings of ~3·2 Å and it was assumed that these represent elements of the rutile structure, viewed along $\mathbf{c}_{rut}$. The framework of octahedral linkages shown in Fig. 4(*a*) was then drawn. This shows hollandite-type tunnels surrounded by pairs of edge-shared octahedra and linked together by elements of the rutile structure. The remaining space was then filled by drawing in extensions of the β-gallia-type structure surrounding the hollandite-type tunnels as shown in Fig. 4(*b*), using the theoretical principles discussed earlier, see Bursill (1979*a*). The β-gallia units naturally adopt two orthogonal orientations with respect to the tunnels, giving rise to glide planes parallel to 19·1 Å cell edges. The space group was thereby deduced to be *P*4/*n* (No. 85). A complete structural model was then drawn using the known atomic coordinates for the hollandite, rutile and β-gallia elements of the structure (Fig. 5). The atomic coordinates for the asymmetric unit were then calculated and these were used for computer simulation of the images. Our image calculation techniques have been described previously (MacLagan, Bursill & Spargo, 1977; Bursill & Wilson, 1977). Figs. 2(*c*,*d*) show the image matches obtained for the thin edge (*c*) and also a thicker area of crystal (*d*). (The relevant electron-optical parameters are given in the caption.) It is clear that the derived structure (Fig. 5) does provide excellent agreement with these observations. It was also possible to obtain reasonable image matches for Fig. 3(*a*) to (*d*). However, it became clear that the simple PCDA does not apply for the experimentally achieved conditions. Thus there is no true minimim-contrast condition and, consequently, a simple reversal of contrast cannot be observed by changing the sign of Δf. In addition the through-focal computed images showed that there was not a simple progression from Fig. 3(*b*) ($\Delta f = -610$ Å) to Fig. 3(*c*) ($\Delta f = -250$ Å), as expected according to the PCDA. Rather, contrast differences comparable to those shown in Fig. 3(*a*,*d*) occur for $\Delta f = -450$ Å. A close study of the transmitted amplitudes and phases of the beams leaving the crystal showed that the crystal potentials for this material are too large to allow a true PCD image to be obtained, even for a crystal of thickness < 10 Å. Nevertheless, it would seem that the 'optimally defocused' image (Fig. 3*c*) did provide a reliable, albeit fortuitous, structural model which was in good agreement with the observed thickness and defocus variations of the image intensity.

The stoichiometry of the structure may be deduced from Fig. 5 by assuming that Ga occupies the edge-shared octahedral and the tetrahedrally coordinated sites characteristic of β-gallia, that Ti occupies the octahedrally coordinated sites in the rutile-like columns, and that Ba occupies the eight-coordinated sites in the hollandite-like tunnels. For tunnel occupancy $\frac{1}{2}$ we obtain $BaTi_6Ga_{12}O_{31}$, assuming all cations have maximum oxidation states. However, we note that, in general, Ti may substitute for Ga in the edge-shared octahedral sites so that if the tunnel occupancy (x) is allowed to vary we obtain $Ba_xTi_{8-2x}Ga_{10+2x}O_{31}$, where the maximum extent of x is $0{\cdot}0 < x < 2{\cdot}0$. Further studies of the stabiiity range of this phase, and of any possible ordering of Ba along the tunnels (*i.e.* along **c**), and of the isomorphous phase $Ba_xTi_{8-x}Mg_{10+x}O_{31}$, are in progress.

This work was financially supported by the Australian Research Grants Committee and the University of Melbourne. The assistance of Mr R. Glaisher, with the image calculations, is gratefully acknowledged.

References

BURSILL, L. A. (1979*a*). *Acta Cryst.* B**35**, 530–538.

BURSILL, L. A. (1979*b*). *Acta Cryst.* A**35**, 449–458.

BURSILL, L. A. (1979*c*). *Direct Imaging of Atoms in Crystals and Molecules*. Nobel Symp. No. 47, Lidingo; *Chem. Scr.* **14**, 83–97.

BURSILL, L. A. & GRZINIC, G. (1980). *Acta Cryst.* B**36**, 2902–2913

BURSILL, L. A., SPARGO, A. E. C., WENTWORTH, D. & WOOD, G. J. (1979). *J. Appl. Cryst.* **12**, 279–286.

BURSILL, L. A. & WILSON, A. R. (1977). *Acta Cryst.* A**33**, 672–676.

COWLEY, J. M. (1975). *Diffraction Physics*, p. 60. New York: North-Holland.

LYNCH, D. F., MOODIE, A. F. & O'KEEFE, M. A. (1975). *Acta Cryst.* A**31**, 300–307.

MACLAGAN, D. S., BURSILL, L. A. & SPARGO, A. E. C. (1977). *Philos. Mag.* **35**, 757–780.

SCHERZER, O. (1949). *J. Appl. Phys.* **20**, 20–29.

SPENCE, J. H. C., O'KEEFE, M. A. & IIJIMA, S. (1978). *Philos. Mag.* **38**, 463–482.

SPENCE, J. H. C., O'KEEFE, M. A. & KOLAR, J. (1977). *Optik*, **49**, 307–323.

WILSON, A. R., BURSILL, L. A. & SPARGO, A. E. C. (1979). *Optik*, **52**, 313–336.

Acta Cryst. (1980). B**36**, 2902–2913

Incommensurate Superlattice Ordering in the Hollandites $Ba_xTi_{8-x}Mg_xO_{16}$ and $Ba_xTi_{8-2x}Ga_{2x}O_{16}$

BY L. A. BURSILL* AND G. GRZINIC

Department of Physical Chemistry, Lensfield Road, Cambridge CB2 1EP, England

(*Received* 17 *December* 1979; *accepted* 15 *August* 1980)

Abstract

Electron diffraction studies revealed a continuous variation of superlattice periodicity $m \times d_{002}$ with changes in stoichiometry x of the hollandite phases $Ba_xTi_{8-x}Mg_xO_{16}$ and $Ba_xTi_{8-2x}Ga_{2x}O_{16}$ with $4{\cdot}70 < m < 5{\cdot}93$ for $0{\cdot}80 < x < 1{\cdot}33$. The superlattice only becomes commensurate for $x = 1{\cdot}20$ ($m = 5{\cdot}00$). High-resolution (3 Å) electron microscope images and computer-simulation techniques were used to determine the short-range ordered arrangements of Ba^{2+} ions within the tunnels of the MX_2 framework of the hollandite structure. Three basic structures were found, for $x = 0{\cdot}80$, $1{\cdot}20$ and $1{\cdot}33$, and the incommensurate periodicities explained in terms of intergrowths of these three plus small elements of an $m = 2$ structure. The origin of the range of incommensurate spacings is discussed in terms of electrostatic repulsions between Ba^{2+} ions and the observed softening of the Λ_5 transverse acoustic mode of rutile (TiO_2) for $m = 6$. Diffusion mechanisms for ionic conductivity in hollandites are briefly discussed but it is clear that the observations and analysis presented here explain why hollandites gave very disappointing results when used as solid electrolytes even though dielectric measurements suggested a relatively low activation energy ($0{\cdot}17$ eV) for Ba^{2+} ion hopping. In fact the structural models used previously and the corresponding interpretations of dielectric absorption measurements were based on oversimplifications of the real structures.

* On leave from: School of Physics, The University of Melbourne, Parkville, Victoria 3052, Australia.

0567-7408/80/122902-12$01.00